ImmunoHorizons

RESEARCH ARTICLE | OCTOBER 29 2021

PRMT5 Promotes Symmetric Dimethylation of RNA Processing Proteins and Modulates Activated T Cell Alternative Splicing and Ca^{2+}/NFAT Signaling

Shouvonik Sengupta; ... et. al

Immunohorizons (2021) 5 (10): 884–897.
https://doi.org/10.4049/immunohorizons.2100076

ImmunoHorizons

RESEARCH ARTICLE

Adaptive Immunity

PRMT5 Promotes Symmetric Dimethylation of RNA Processing Proteins and Modulates Activated T Cell Alternative Splicing and Ca^{2+}/NFAT Signaling

Shouvonik Sengupta,[*,†] Kelsi O. West,[‡] Shridhar Sanghvi,[§,¶] Georgios Laliotis,[‖] Laura M. Agosto,[#] Kristen W. Lynch,[#] Philip N. Tsichlis,[,††] Harpreet Singh,[§] Kristin L. Patrick,[‡] and Mireia Guerau-de-Arellano[*,‡‡,§§,¶¶]**

*School of Health and Rehabilitation Sciences, The Ohio State University, Columbus, OH; [†]Biomedical Sciences Graduate Program, The Ohio State University, Columbus, OH; [‡]Department of Microbial Pathogenesis and Immunology, Texas A&M Health Science Center, Bryan, TX; [§]Department of Physiology and Cell Biology, The Ohio State University, Columbus, OH; [¶]Molecular, Cellular, and Developmental Biology Graduate Program, The Ohio State University, Columbus; [‖]Department of Oncology, Johns Hopkins University, Baltimore, MD; [#]Department of Biochemistry and Biophysics, University of Pennsylvania, Philadelphia, PA; **Department of Cancer Biology and Genetics, The Ohio State University, Columbus, OH; [††]The Ohio State University Comprehensive Cancer Center, Columbus, OH; [‡‡]Institute for Behavioral Medicine Research, The Ohio State University, Columbus, OH; [§§]Department of Microbial Infection and Immunity, The Ohio State University, Columbus, OH; and [¶¶]Department of Neuroscience, The Ohio State University, Columbus, OH

ABSTRACT

Protein arginine methyltransferase (PRMT) 5 is the type 2 methyltransferase catalyzing symmetric dimethylation of arginine. PRMT5 inhibition or deletion in CD4 Th cells reduces TCR engagement-induced IL-2 production and Th cell expansion and confers protection against experimental autoimmune encephalomyelitis, the animal model of multiple sclerosis. However, the mechanisms by which PRMT5 modulates Th cell proliferation are still not completely understood, and neither are the methylation targets in T cells. In this manuscript, we uncover the role of PRMT5 on alternative splicing in activated mouse T cells and identify several targets of PRMT5 symmetric dimethylation involved in splicing. In addition, we find a possible link between PRMT5-mediated alternative splicing of transient receptor potential cation channel subfamily M member 4 (*Trpm4*) and TCR/NFAT signaling/IL-2 production. This understanding may guide development of drugs targeting these processes to benefit patients with T cell–mediated diseases. *ImmunoHorizons*, 2021, 5: 884–897.

Received for publication August 11, 2021. Accepted for publication October 1, 2021.

Address correspondence and reprint requests to: Mireia Guerau-de-Arellano, The Ohio State University, 453 W. 10th Avenue, Room 535C, Columbus, OH 43210. E-mail address: mireia.guerau@osumc.edu

ORCIDs: 0000-0003-1680-1315 (S. Sengupta); 0000-0002-9632-7205 (K.O.W.); 0000-0001-9254-7078 (S. Sanghvi); 0000-0001-9205-8258 (G.L.); 0000-0003-0271-6574 (L.M.A.); 0000-0002-5300-0448 (P.N.T.); 0000-0002-6135-1897 (H.S.); 0000-0003-2442-4679 (K.L.P.); 0000-0002-0600-4593 (M.G.-d.-A.)

This work was supported by National Institutes of Health (NIH)/National Institute of Allergy and Infectious Diseases Grants R01AI121405 and 1R21AI127354 (both to M.G.d.A.), start-up funds from The Ohio State University School of Health and Rehabilitation Sciences (to M.G.d.A.), an American Association of Immunologists Travel for Techniques Award (to M.G.d.A. and S. Sengupta), the Comprehensive Cancer Center Mass Spectrometry Resource (Core Cancer Center Support Grant S10OD018056), NIH/National Cancer Institute Grant 01-CA186729 (to P.N.T.), a Pelotonia postdoctoral fellowship (to G.L.), and the National Center for Advancing Translational Sciences, which sponsors the Center for Clinical and Translational Science Award (Grant UL1TR002733). The content is the sole responsibility of the authors and does not necessarily represent the official views of the National Center for Advancing Translational Sciences or the NIH.

The RNA sequencing data in resting T cells associated with the RNA sequencing experiment have been submitted to the Gene Expression Omnibus (https://www.ncbi.nlm.nih.gov/geo/) under accession number GSE181931.

Abbreviations used in this article: Ψ, expected percent spliced value; $\Delta\Psi$, expected change in Ψ; AJ, alternative junction; AS, alternative splicing; EAE, experimental autoimmune encephalomyelitis; GO, Gene Ontology; IP, immunoprecipitation; KO, knockout; LC-MS/MS, liquid chromatography/tandem MS; LSV, local splice variant; MAJIQ, modeling alternative junction inclusion quantification; MS, mass spectrometry; MS/MS, tandem mass spectrometry; PRMT, protein arginine methyltransferase; RNA-Seq, RNA sequencing; SDM, symmetric dimethylation, symmetrically dimethylated; sh, short hairpin; SL, stem loop; snRNA, small nuclear RNA; Trpm4, transient receptor potential cation channel subfamily M member 4.

The online version of this article contains supplemental material.

https://doi.org/10.4049/immunohorizons.2100076

ImmunoHorizons is published by The American Association of Immunologists, Inc.

INTRODUCTION

Arguably, CD4 Th cells play one of the most critical roles in immunity by orchestrating Ag-specific adaptive immunity and enhancing innate immunity via release of cytokines (1). The resulting cytokine gradient elicits autocrine and paracrine effects on CD4 Th cells, CD8 T cytotoxic cells, B cells, and myeloid cells. Therefore, a lack of CD4 Th cells substantially impacts both humoral and cytotoxic immune responses and commonly results in life-threatening infections. In turn, overreactive CD4 Th cell responses can lead to the chronic inflammation and tissue destruction observed in autoimmune disease. Protein arginine methyltransferase (PRMT) 5 is a type II methyltransferase that catalyzes symmetric dimethylation (SDM) of protein arginines and plays an important role in development and cancer. Previous work from our laboratory and others has shown that PRMT5 is induced after CD4 Th cell activation/autoimmune responses and that loss of PRMT5 reduces TCR engagement-induced Th cell expansion and confers protection against the mouse model of multiple sclerosis, experimental autoimmune encephalomyelitis (EAE) (2–4). However, the methylation targets of PRMT5 in T cells and associated molecular mechanisms are not well defined (5).

A key step for protective immune or pathogenic autoimmune responses is the clonal expansion of Ag-specific T cells induced by TCR engagement (6). TCR engagement activates signaling pathways (7) that lead to NFAT activation (8) and cell cycle progression (9). NFAT activation results in nuclear localization, activation of the IL-2 promoter, and IL-2 cytokine transcription (10). Once secreted, IL-2 binds the IL-2R in an autocrine and paracrine manner and promotes T cell growth and proliferation (11). We have previously seen that PRMT5 can promote IL-2 production, cell cycle progression (12), and T cell proliferation (2). However, the impact of PRMT5 loss on TCR/NFAT signaling that leads to IL-2 production and T cell proliferation remains unexplored.

As a consequence of TCR signaling, T cells undergo dramatic changes in their gene expression programs. These changes support the transition from naive to highly proliferating and cytokine-producing effector T cells. A substantial portion of gene expression modulation occurs at the gene expression level. However, additional modulation is possible via alternative splicing (AS) (13). AS is the process by which exons are included or excluded in the final processed mRNA transcript, resulting in distinct isoforms from the same gene (14). AS therefore provides an important layer of gene expression programming control by diversifying the proteins that are actually encoded within genes. Previous work from the Lynch laboratory (13, 15, 16) has established that antigenic/TCR stimulation modulates the AS gene expression pattern of T cells, as revealed by RNA sequencing (RNA-Seq), quantitative microarray, bioinformatics, and RT-PCR analyses. The resulting protein isoforms have been linked to functional outcomes, such as TCR α-chain transcription (17), TCR signal transduction (18), and JNK–CELF2–dependent splicing control (19), indicating AS plays crucial functional roles in activated T cell biology. PRMT5 plays a role in splicing via SDM of spliceosome Sm protein components, such as SMB, SMB′, SMD1, and SMD3 (20–25). A conserved role for PRMT5 in methylation of spliceosome Sm proteins and splicing was initially established in plant and insect models (22, 26, 27), whereas studies in mouse stem cell and human cancer cell line models show that PRMT5's impact on constitutive and AS is conserved to mammals (28–31). For example, a study by the Guccione group (28) showed that the absence of PRMT5 in neural stem progenitor cells leads to defects in the core splicing machinery and reduced constitutive and AS of genes with weak 5′ donor sites (29). However, genetic evidence that PRMT5 is involved in physiological T cell splicing is lacking.

In this manuscript, we explore the specific role of PRMT5 on AS changes induced after T cell activation, methylation targets of PRMT5 in T cells involved in splicing, and potential links between a specific AS *Trpm4* isoform and altered TCR/NFAT signaling. We find that PRMT5 deletion alters the AS pattern induced by T cell activation and results in the loss of SDM of proteins involved in splicing, such as SMDs, SNRPA1, and HNRNPK. We also report specific validated changes in the AS of *Trpm4*, a Ca^{2+} responsive Na^{+} channel that plays an important role in total calcium processing and NFAT-dependent IL-2 production in Th cells. Overall, these data conclusively link PRMT5 to TCR-induced AS in T cells and suggest that altered methylation in splicing proteins and changes in Ca^{2+}/NFAT signaling underlie TCR expansion defects in PRMT5-deficient T cells.

MATERIALS AND METHODS

Mice

Age-matched 9- to 13-wk-old iCD4-PRMT5$^{fl/fl}$ (CD4creER^{-}PRMT5$^{fl/fl}$) and iCD4-PRMT5$^{\Delta/\Delta}$ (CD4creER^{+}PRMT5$^{fl/fl}$) mice, described in Webb et al. (3), on the C57BL/6 background were used for RNA-Seq and mass spectrometry (MS). Age-matched 9- to 13-wk-old C57BL/6 background constitutive T-PRMT5$^{fl/fl}$ (CD4cre^{-}PRMT5$^{fl/fl}$) and T-PRMT5$^{\Delta/\Delta}$ (CD4cre^{+}PRMT5$^{fl/fl}$) mice, also described in Webb et al. (3), were used in the remainder of experiments. Males and females were used in experiments, and no significant differences were observed between genders. Animal use procedures were approved under Institutional Animal Care and Use Committee protocol number 2013A00000151-R1. All animals were euthanized under the American Veterinary Medical Association guidelines.

Deletion of PRMT5 and murine CD4 Th cell isolation in vivo tamoxifen treatment

iCD4-PRMT5$^{fl/fl}$ and iCD4-PRMT5$^{\Delta/\Delta}$ mice were administered 300 mg/kg (7.5 μl/g) tamoxifen (catalog no. T5648; Sigma-Aldrich) by gavage for 5 d and euthanized 2 d after the last dose for secondary lymphoid organ (lymph nodes and spleen) harvest. Deletion of PRMT5 in T cells did not require

https://doi.org/10.4049/immunohorizons.2100076

tamoxifen treatment in T-PRMT5$^{fl/fl}$ (CD4cre^{-}PRMT5$^{fl/fl}$) and T-PRMT5$^{\Delta/\Delta}$ (CD4cre^{+}PRMT5$^{fl/fl}$) mice. Harvested organs were processed to a cell suspension and subsequently used for CD4 Th cell isolation. Murine CD4 T cells were isolated from processed lymphoid organs using EasyEights Magnet (catalog no. 18103, Stem Cell Technologies) and the whole CD4^{+} T Cell Isolation Kit (catalog no. 19852; Stem Cell Technologies). Purity of CD4 T cells was in the range of 87–95%, as measured by flow cytometry. Additional details on the tamoxifen treatment regimen and mouse immunological parameters after tamoxifen treatment can be found in Webb et al. (3).

Cell culture

T cells were cultured in EAE media (RPMI 1640 plus 10% FBS plus 2mM L-glutamine plus 1:100 penicillin–streptomycin plus 1mM sodium pyruvate plus 1:100 minimal essential amino acids plus 13mM HEPES plus 1:500 2-ME). Unless otherwise indicated, CD4 T cells were activated on coated 5 μg/ml CD3 and soluble 2 μg/ml CD28 for 48 h in 24-well plates. Human Jurkat T cells with a stable *PRMT5* knockdown were generated by the Tsichlis laboratory (3) at OSU, as previously described. Briefly, pLx304 DEST EV was used as an empty vector control cell line (termed EV) and PRMT5 short hairpin (sh) RNA (catalog no. SHCLNG-NM_006109, clone ID TRCN0000107085; MilliporeSigma) was used to induce the PRMT5 knockdown cell line (termed shPRMT5). Cells were cultured in standard Jurkat cell culture media (American Type Culture Collection) for 24–48 h until desired confluency was reached prior to downstream processing.

RNA-Seq

Whole CD4^{+} T cells from iCD4-PRMT5$^{fl/fl}$ and iCD4-PRMT5$^{\Delta/\Delta}$ mice (n = 3 pooled mice per sample and n = 3 samples per group) were used for RNA-Seq. Samples were either lysed directly ex vivo (resting) or activated (anti-CD3/CD28, no cytokines, 48 h) before lysis and RNA isolation. RNA isolation was done with the Direct-zol RNA MiniPrep Kit (catalog no. R2052; Zymo Research) according to the manufacturer's instructions. A total of 1 ng of total RNA was used for quality control, library preparation, and RNA-Seq. Quality of RNA was evaluated using the Agilent 2100 Bioanalyzer and RNA Nano Chips (Agilent Technologies). Samples with RNA integrity number greater than 7.7 were considered for sequencing. Data pertaining to activated and resting T cells associated with the RNA-Seq experiment can be found in National Center for Biotechnology Information's Gene Expression Omnibus (https://www.ncbi.nlm.nih.gov/geo/) under the accession numbers GSE141168 and GSE181931, respectively. For additional information on RNA-Seq run and analysis, refer to the protocol listed in Webb et al. (3). RNA-Seq was performed by the Genomic Services Laboratory of the Abigail Wexner Research Institute at Nationwide Children's Hospital, Columbus, Ohio.

Modeling Alternative Junction Inclusion Quantification and Voila

AS events were analyzed using modeling alternative junction inclusion quantification (MAJIQ) and Voila under default parameters (32). PRMT5$^{fl/fl}$ mice T cell FastQ files were set as the control group to compare PRMT5$^{\Delta/\Delta}$ files against. In brief, raw junction spanning reads from RNA-Seq FastQ files were aligned to the GRCm38.p3 assembly of the *Mus musculus* reference from the National Center for Biotechnology Information using STAR RNA-Seq aligner (2.6.0c). These alignments were fed into MAJIQ to construct splice graphs for transcripts using the RefSeq annotation and identify both known and novel AS events in the dataset. All identifiable local splice variants (LSVs) were analyzed from the splice graphs with minimum reads set to at least 10 to pass the quantifiable threshold. For each exonic–intronic junction in an LSV, MAJIQ quantified the expected percent spliced value (Ψ) in PRMT5$^{fl/fl}$ and iCD4-PRMT5$^{\Delta/\Delta}$ T cell samples and the expected change in Ψ ($\Delta\Psi$) between PRMT5$^{fl/fl}$ and iCD4-PRMT5$^{\Delta/\Delta}$ T cell samples. The Voila results were processed with a filter of at least 20% to include high-confidence changing LSVs (at least two junctions with a 95% probability of expected $\Delta\Psi$ of at least an absolute value of 20 Ψ units ($\Delta\Psi \geq/\leq 20$) between iCD4-PRMT5$^{fl/fl}$ and iCD4-PRMT5$^{\Delta/\Delta}$ T cell samples. The high-confidence results were further classified into exon skipping, alternative 5′, alternative 3′ splice site or intron retention events.

Semiquantitative PCR

To evaluate mRNA expression, 200–300 ng of RNA was reverse transcribed using oligo d(T) or random primers and Superscript III First-Strand Synthesis System (catalog no. 18080051; Thermo Fisher Scientific) according to the manufacturer's instructions. Samples were run on a Mastercycler Nexus (Eppendorf). Exon 20 region-specific primers spanned from exon 19 to exon 21 (forward: 5′-TCCTCTTCTTCCTCTG-CGTG-3′; reverse: 5′-ATTCCCGGATGAGGCTGTAG-3′; products e20 skipped band, 230 bp and e20 included band, 408 bp). Control primers were on exon 19 (forward: 5′-CCTCT-TCTTCCTCTGCGTGT-3′, reverse: 5′-ATTTCCTCCTGGGGA-ATTTG-3′; product, 150 bp). An initial denaturation step at 95°C for 5 min was followed by 30 cycles of denaturation at 95°C for 30 s, annealing at 54°C for 1 min, and extension at 72°C for 30 s. PCR products were run on 1.5% agarose gels with 0.5% TBE buffer. e20 skipped PCR products were confirmed by use of nested primers (forward: 5′-GCC CTC ATG ATT CCA GGT AA-3′; reverse: 5′-TCC AGT AGA GGT CGC TGT TG-3′), and Sanger sequencing was performed at the Ohio State University Comprehensive Cancer Center genomic shared resources.

Assessment of calcium signaling in T cells

Isolated activated (anti-CD3/CD28, 2.5 μg/ml, 50 U IL-2, 48 h) CD4^{+} T cells from PRMT5$^{fl/fl}$ and T-PRMT5$^{\Delta/\Delta}$ mice were plated on poly-L-lysine (catalog no. P8920-100ML;

MilliporeSigma) –coated glass-bottom dishes (Cellvis 35-mm–14-mm microwell number 1.5 cover glass; catalog no. NC0794151; Thermo Fisher Scientific) for 120 min. Cells were then treated with 10 μmol Fluo-4 AM (catalog no. F14201; Invitrogen) dye for 30 min in DMEM (without phenol red and glutamine; catalog no. 11054020; Thermo Fisher Scientific) at 5% CO_2 in a humidifying incubator at 37°C. The dye was then washed out, and cells were incubated for 30 min in modified EAE media supplemented with 10% FBS for de-esterification. Following de-esterification, cells were switched to modified Ringer solutions with 0 mM Ca^{2+} (120 mM NaCl, 5 mM KCl, 1 mM $MgCl_2$, 25 mM $NaHCO_3$, and 5.5 mM D-glucose [pH 7.3]) for imaging with a Nikon A1R HD laser-scanning confocal microscope. Fluo-4 was excited using a 488-nm laser, and fluorescence emission was detected at 500–550 nm. Resting Ca^{2+} baseline was recorded for 150 s prior to addition of sarcoplasmic reticulum Ca^{2+}–ATPase inhibitor thapsigargin (2 μM). After 150 s $CaCl_2$ (2mM) was added, and calcium uptake was monitored for 600 s. The data are represented as $\Delta F/F_0$ versus time, where F_0 is basal fluorescence and $\Delta F = F - F_0$.

Immunocytochemistry

Isolated activated (5 μg/ml anti-CD3 and soluble 2 μg/ml CD28, 48 h) $CD4^+$ T cells from $PRMT5^{fl/fl}$ and T-$PRMT5^{\Delta/\Delta}$ mice were plated on poly-L-lysine (catalog no. P8920-100ML; MilliporeSigma)–coated glass cover slips for 120 min. Cells were then stained with wheat germ agglutinin for 10 min prior to fixing with 4% paraformaldehyde (catalog no. 15713; Electron Microscopy Sciences) for 10 min and permeabilization with 0.5% Triton X-100 for 10 min. Samples were blocked with 10% normal goat serum for 10 min and incubated in NFATc1 Ab (catalog no. sc-7294; Santa Cruz Biotechnology) overnight at 4°C. Samples were then incubated in secondary Ab conjugates Atto 647N (1 μg/ml each of anti-mouse; catalog no. 50185-1ML-F; Sigma-Aldrich) for 60 min, followed by 10.9 mM DAPI (1:10,000) (catalog no. D9542; Sigma-Aldrich) staining for 10 min. Coverslips were mounted with ProLong Gold Antifade Mountant (catalog no. P36930; Invitrogen) and cells were imaged with Nikon A1R high-resolution confocal microscopy. NFAT and nuclear stain colocalization index (33) was calculated using ImageJ. The Pearson R value with no threshold condition was selected for the calculation of colocalization index.

Flow cytometry

For flow cytometry, 48-h activated T cells from $PRMT5^{fl/fl}$ and T-$PRMT5^{\Delta/\Delta}$ mice were fixed with 4% paraformaldehyde (catalog no. 15713; Electron Microscopy Sciences) for 10 min in V-bottom plates (catalog no. 3897; Costar). Samples were blocked with 5% normal goat serum for 1 h and incubated in anti-TRPM4 (catalog no. ab106200; Abcam) or normal mouse IgG (catalog no.sc-2025; Santa Cruz Biotechnology) Abs overnight. Samples were then incubated in goat anti-rabbit IgG Alexa Fluor 488–conjugated (catalog no. ab150085; Abcam) secondary Abs for 60 min on the next day prior to washing and running on FACSCalibur with DxP multicolor upgrades (Cytek). Analysis was performed using FlowJo v10.

Cytokine ELISA

IL-2 cytokine in 48-h supernatants of activated T cells from $PRMT5^{fl/fl}$ and T-$PRMT5^{\Delta/\Delta}$ mice was analyzed by sandwich ELISA. Murine IL-2 ELISA capture (catalog no. 14-7022-85; Thermo Fisher Scientific) and detection (catalog no. 13-7021-85; Thermo Fisher Scientific) Ab reagents were purchased from Invitrogen/eBioscience. The capture Ab was coated overnight at 2 μg/ml in coating buffer (0.1M $NaHCO_3$ [pH 9.5]). On the following day, plates were washed with 0.1% PBS/Tween-20 solution and blocked with 1% BSA/PBS for 2 h. Following blocking, 100 μl of IL-2 standard (catalog no. 14-8021-64; Invitrogen/eBioscience) or supernatants are added to the wells. Plates were incubated overnight at 4°C, and the following day, plates were washed with 0.1% PBS/Tween-20 solution, and 100 μl of detection Ab diluted in 1% BSA/PBS was added to the wells for 60 min, followed by 2.5 μg/ml Avidin peroxidase prepared in 1% BSA/PBS for 30 min. After washes, 0.1% H_2O_2/ABTS was added to the wells, and the developed color signal was read at 405 nm on the SpectraMax Plus 384 microplate reader (Molecular Devices) at 2–15 min.

Mass spectrometry

Isolated resting and activated (anti-CD3/CD28, no cytokines, 2 d) $CD4^+$ T cells from iCD4-$PRMT5^{fl/fl}$ and iCD4-$PRMT5^{\Delta/\Delta}$ mice ($n = 3$ pooled mice per sample; $n = 3$ samples per group) were lysed in our in-house lysis buffer (50 mM triethylammonium bicarbonate, catalog no. T7408-500ML; MilliporeSigma; plus 0.05% *n*-Dodecyl-β-D-maltoside, catalog no. D4641-1G; MilliporeSigma). Protein was quantified using the Pierce BCA Kit (catalog no.23225; Thermo Fisher Scientific), and 30 μg was used for immunoprecipitation (IP). IP with the SYM10 Ab (catalog no.07-412; MilliporeSigma) was done according to manufacturer's instructions using the Pierce Protein A/G Magnetic Beads (catalog no.88802; Thermo Fisher Scientific). Liquid chromatography/tandem MS (LC-MS/MS) was performed on IP samples using an Orbitrap Fusion Mass Spectrometer equipped with an EASY-Spray Sources operated in positive ion mode by the Ohio State University Genomics Shared Resource. Samples were separated on an EASY-Spray nano column (PepMap RSLC, C18 3μ 100A, 75 μm ×150 mm; Thermo Fisher Scientific) using a two-dimensional RSLC high-performance liquid chromatography system from Thermo Fisher Scientific. Each sample was injected into the μ-Precolumns Cartridge (Thermo Fisher Scientific) and desalted with 0.1% formic acid in water for 5 min. The injector port was then switched to inject the sample, and the peptides were eluted off of the trap onto the column. Mobile phase A was 0.1% formic acid in water, and acetonitrile (with 0.1% formic acid) was used as mobile phase B. The flow rate was set at 300 nl/min, mobile phase A was 0.1% formic acid in water, and acetonitrile (with 0.1% formic acid) was used as mobile phase B. Flow rate was set at 300 nl/min. Typically, mobile phase B was

https://doi.org/10.4049/immunohorizons.2100076

increased from 2 to 35% to 55% in 125 and 23 min and then increased from 55 to 90% in 10 min and then kept at 95% for another 5 min before being brought back quickly to 2% in 2 min. The column was equilibrated at 2% of mobile phase B (or 98% A) for 15 min before the next sample injection. MS/MS data were acquired with a spray voltage of 1.7 kV, and a capillary temperature of 275°C was used. The scan sequence of the mass spectrometer was based on the preview mode data-dependent TopSpeed method; the analysis was programmed for a full scan recorded between m/z 375 – 1700 and an MS/MS scan to generate product ion spectra to determine amino acid sequence in consecutive scans starting from the most abundant peaks in the spectrum in the next 3 s. To achieve high mass accuracy MS determination, the full scan was performed at Fourier transform mode and the resolution was set at 120,000. EASY-IC was used for internal mass calibration. The automatic gain control target ion number for Fourier transform full scan was set at 4×10^5 ions, maximum ion injection time was set at 50 ms, and microscan number was set at 1. Multistage MS was performed using ion trap mode to ensure the highest signal intensity of MSn spectra using both higher-energy C-trap dissociation methods (30%). The automatic gain control target ion number for ion trap MSn scan was set at 10000 ions, maximum ion injection time was set at 30 ms and the microscan number was set at 1. Dynamic exclusion is enabled with a repeat count of 1 within 60 s and a low mass width and high mass width of 10 ppm.

MS analyses

Label-free quantitation (34) was performed using the spectral count approach, in which the relative protein quantitation is measured by comparing the number of MS/MS spectra identified from the same protein in each of the multiple LC-MS/MS datasets. Scaffold (Proteome Software, Portland, OR) was used for data analysis. Results were filtered with 95% confident level first. Only proteins that pass 1% false discovery rate and have a minimal of two unique peptides were considered as valid identification.

Western blotting and IP

Activated whole $CD4^+$ T cells and Jurkat cells were pelleted and frozen at −80°C. Samples were lysed in RIPA buffer (10 mM Tris [pH 7.4], 150 mM NaCl, 1% Triton X-100, 0.1% SDS, 1% deoxycholate) for Western blotting and IP lysis buffer for IP (50 mM Tris, 150 mM NaCl, 1% NP-40, 0.1% Triton X-100, 0.5% sodium deoxycholate). A total of 4–10 μg of protein was run for the Western blot, and 40–50 μg of initial protein was used for IP. Input samples were loaded as 10% of IP protein loading. Samples were run on 7.5% SDS-PAGE gels and transferred onto nitrocellulose membranes. Blots were blocked with 1% milk protein in TBS–Tween (0.1%). IP was performed according to the manufacturer's instructions provided by Santa Cruz Biotechnology. IP Abs used were hnRNP K (catalog no. ab39975; Abcam) and normal mouse IgG (catalog no. sc-2025; Santa Cruz Biotechnology). Protein A/G PLUS-Agarose beads were used for the pull-down (catalog no. sc-2003; Santa Cruz Biotechnology). Additional information on protein isolation, Western blotting, IP, and blot imaging procedures can be found in Webb et al. (3).

Statistics

Statistical analyses were done using the GraphPad Prism software (v9). A two-tailed Student *t* test or one-way ANOVA followed by Tukey or Sidak post hoc multiple comparisons test was performed as appropriate. Raw RNA-Seq data were normalized, and postalignment statistical analyses were performed using DESeq2 and custom analysis scripts written in R.

RESULTS

PRMT5 modulates T cell activation-dependent AS

Substantial AS modulation occurs in response to TCR stimulation of Jurkat T cells (15). However, the contribution of PRMT5 to TCR stimulation-dependent AS changes is unknown. To address this, we leveraged our recently developed conditional CD4 T cell–specific PRMT5 knockout (KO) mouse model (3), RNA-Seq, and bioinformatics tools to identify and analyze AS events. We isolated purified CD4 Th cells from iCD4-$PRMT5^{fl/fl}$ and iCD4-$PRMT5^{\Delta/\Delta}$ mice in resting versus anti-CD3/CD28–activated conditions (henceforth referred to as activated) for paired-end RNA-Seq (Fig. 1A). Detection, quantification, and visualization of LSVs from RNA-Seq data were then achieved with the MAJIQ and Voila software packages created in the Barash laboratory (32). MAJIQ software is, in theory, capable of detecting any splicing events involving two or more junctions, including not previously annotated splicing events.

We first used MAJIQ to evaluate AS changes occurring as a consequence of primary murine CD4 Th cell activation in control, PRMT5-sufficient T cells. We tuned our analysis to identify the LSVs (defined as all possible splits in the exon boundary that have events), alternative junctions (AJs; defined as LSVs with two or more junctions having 20–80% of reads coming into/going out of the junction being considered) and the genes in which these AS changes occurred. MAJIQ identified 9071 AJs corresponding to 3649 events impacting 1921 genes (Fig. 1B) upon activation of primary CD4 Th cells (comparing resting versus activated $PRMT5^{fl/fl}$ T cells). Next, we evaluated whether the AS pattern observed in activated T cells was altered by PRMT5 deletion (comparing activated $PRMT5^{fl/fl}$ versus $PRMT5^{\Delta/\Delta}$ T cells). We observed that PRMT5 loss in activated T cells resulted in changes in 2590 AJs corresponding to 857 splicing events over 503 genes (Fig. 1C). These results indicate that PRMT5 regulates an important portion (∼16%) of the activated T cell AS gene expression profile.

To determine how much and in which direction PRMT5 alters splicing, we performed a $\Delta\Psi$ (expected change in Ψ) analysis. Some AJs (38%, or 996 AJs) were detected at a similar level between $PRMT5^{fl/fl}$ and $PRMT5^{\Delta/\Delta}$ activated T

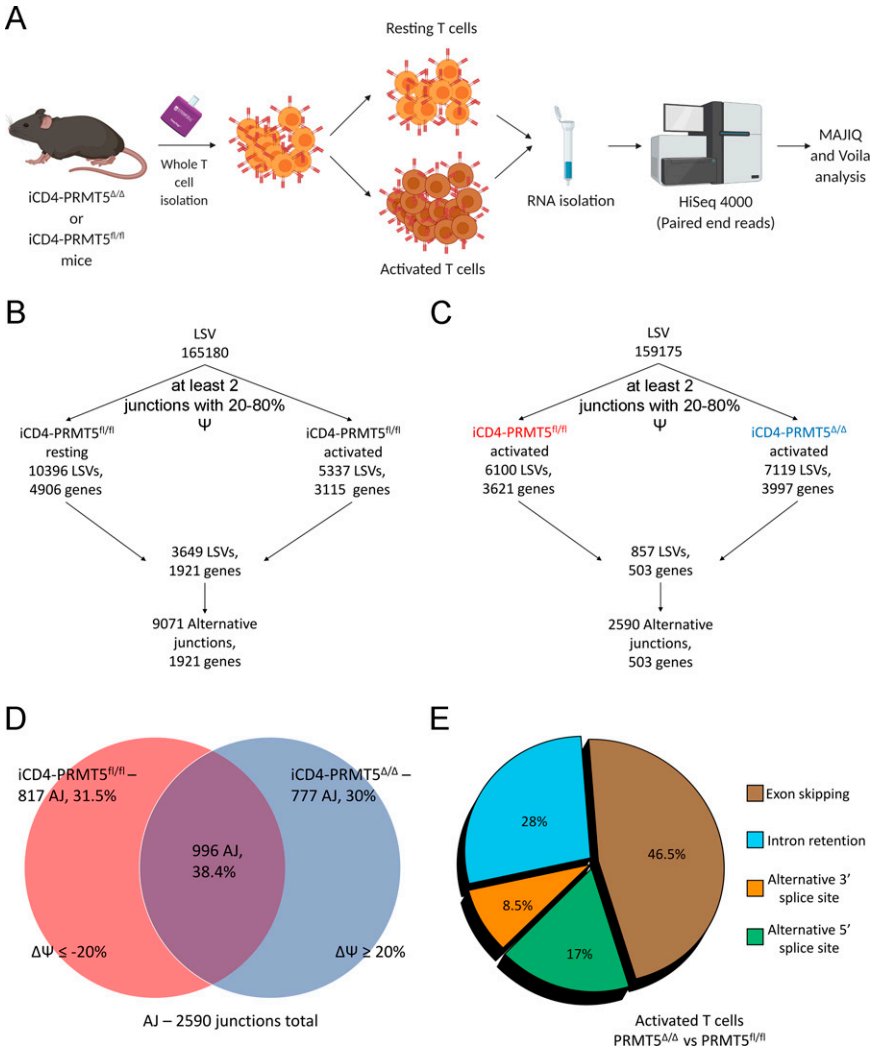

FIGURE 1. MAJIQ analysis reveals novel PRMT5-dependent changes in the AS of 503 genes in T cells.

(**A**) Experimental design for paired-end RNA-Seq of resting and 48-h activated, whole $CD4^+$ T cells isolated from iCD4-$PRMT5^{fl/fl}$ and iCD4-$PRMT5^{\Delta/\Delta}$ mice. $n = 3$ samples combined from nine age-matched mice in each respective group. RNA-Seq was performed on the HiSeq 4000 platform with ~60–80 million reads. Figure created in BioRender. (**B** and **C**) Analysis of LSVs and AJs from MAJIQ. Workflow identifying significantly used AJs by comparing LSVs in resting (B) or 48-h activated (C) iCD4-$PRMT5^{fl/fl}$ or iCD4-$PRMT5^{\Delta/\Delta}$ $CD4^+$ T cells. LSVs with at least two or more exon junctions within the 20–80% spliced index (Ψ) of reads were calculated. A total of 3649 LSVs were observed for the wild-type iCD4-$PRMT5^{fl/fl}$ resting versus iCD4-$PRMT5^{fl/fl}$ activated comparison (B), and 857 LSVs were observed for the iCD4-$PRMT5^{fl/fl}$ activated (red) versus iCD4-$PRMT5^{\Delta/\Delta}$ activated (blue) comparison (C). (**D**) Allocation of LSVs with two or more AJs in iCD4-$PRMT5^{fl/fl}$ act (red) and iCD4-$PRMT5^{\Delta/\Delta}$ act (blue) groups. Shift in AJ usage is denoted as $\Delta\Psi$ and is set at a minimum of 20% between conditions. A total of 817 AJs are $PRMT5^{fl/fl}$ specific, and 777 AJs are $PRMT5^{\Delta/\Delta}$ specific. (**E**) Classification of 503 genes in the iCD4-$PRMT5^{\Delta/\Delta}$ versus $PRMT5^{fl/fl}$ (both activated) comparison from MAJIQ shows most of the AS events belong to exon skipping. Intron retention is the next largest portion of AS changes.

cells. In contrast, ~60% of AJs were used more often in the wild-type $PRMT5^{fl/fl}$ (31.5%, or 817 AJs) or $PRMT5^{\Delta/\Delta}$ (30%, or 777 AJs) condition (Fig. 1D). Finally, we evaluated the distribution of AS type (alternative 5′ or 3′ splice site usage, exon skipping, and intron retention) observed in PRMT5-deficient activated T cells. Among the 2590 AJs modulated by PRMT5, exon skipping (46.5%) was the most frequent with PRMT5 loss, closely followed by intron retention (28%), whereas alternative 5′ or 3′ junctions were less frequent (Fig. 1E).

Similar analyses comparing PRMT5-sufficient versus -deficient T cells in the resting state showed limited AS occurring in resting T cells, with few albeit some differences in AS splicing (408 AJs corresponding to 127 LSVs over 74 genes; Supplemental Fig. 1) existing between resting wild-type versus PRMT5-deficient T cells.

Collectively, these data indicate that the loss of PRMT5 leads to a distinct splicing profile in primary T cells, particularly in activated T cells. This suggests that PRMT5 expression in T cells results in substantial and nonrandom changes in AS, which presumably modulate T cell biology and function. Our results raise the question of how PRMT5 is regulating splicing.

PRMT5 methylates spliceosome Sm/Snrp proteins and the RNA binding protein hnRNP K

PRMT5 has been described as a crucial player in spliceosomal assembly via SDM of Sm proteins (24). However, the spliceosomal or other methylation targets of PRMT5 in T cells are largely unknown. To study this, we first performed an unbiased pull-down of SDM proteins in iCD4-$PRMT5^{fl/fl}$ and iCD4-$PRMT5^{\Delta/\Delta}$ T cells, using the SYM10 Ab that recognizes symmetrically dimethylated RGG and subjected the SDM target-enriched samples to MS (Fig. 2A). We then used the Scaffold software to identify putative methylation targets (Supplemental Table I). PRMT5 is induced at its maximum level at the 48-h time point after T cell activation and contributes to T cell expansion. Therefore, our experimental design used 48-h activated T cells to identify putative PRMT5 methylation targets that modulate activated T cell AS and biology. We expected such targets to be more highly recovered in activated than resting $PRMT5^{fl/fl}$ T cells but less recovered in activated iCD4-$PRMT5^{\Delta/\Delta}$ than activated $PRMT5^{fl/fl}$ T cells. From this, we observed a number of splicing-related proteins that were enriched through SDM Ab pull-down in PRMT5-sufficient but

https://doi.org/10.4049/immunohorizons.2100076

not, or to a lesser extent, in PRMT5-deleted activated T cells. For our analysis, we graphed the raw spectral reads, which are expected to correspond to targets of PRMT5 SDM methylation in T cells.

We found that Sm proteins SMD1, D2, and D3, which are responsible for the Sm ring formation step required for spliceosome formation (35) (Fig. 2 B–D), were recovered significantly less in PRMT5-deficient activated T cells. However, methylated Sm protein recovery was similar between resting and activated wild-type T cells. Recovery of other splicing-related proteins, such as SNRNP70, that helps with spliceosomal assembly (aiding the binding of stem loop (SL) I to U1 small nuclear RNA [snRNA]) (36, 37) or HNRNPA3, which helps with cytoplasmic trafficking of RNA (38), did not significantly decrease with PRMT5 deletion (Fig. 2E, 2F**)**. However, recovery of SNRPA, SNRPA1 (which bind SLII of U1 snRNA and SLIV of U2 snRNA, respectively) and HNRNPK [an RBP that assists in the maturation of precursor mRNAs into mRNAs, stabilizes the mRNA during transport, and controls the translation of the mRNA (39)] followed the expected decrease after PRMT5 loss (Fig. 2 G–I). In addition, HNRNPK recovery followed the expected increase after T cell activation, when PRMT5 is induced, and decreased with PRMT5 deletion (Fig. 2I). Based on this T cell activation and PRMT5-dependent recovery and role of hnRNP K in RNA splicing, we further validated this target in T cells. We performed a "reverse" IP, in which we pulled down the target HNRNPK in activated T cells from iCD4-PRMT5$^{fl/fl}$ and iCD4-PRMT5$^{\Delta/\Delta}$ mice (Fig. 2J) or control versus PRMT5 shRNA-modified human Jurkat T cells (Fig. 2K) and probed with SYM10. Although more total hnRNPK was loaded, similar or less methylated hnRNPK could be detected for samples with PRMT5 loss-of-function condition, resulting in an incomplete but significant reduction of the methylated/total HNRNPK (55 kDa band) ratio in cells from PRMT5 KO murine (Fig. 2J, Supplemental Fig. 2A) and human PRMT5 knockdown (Fig. 2K, Supplemental Fig. 2B, 2C) T cells. Some SDM remained in PRMT5 KO or knockdown conditions, suggesting that other PRMTs that catalyze SDM may provide compensatory methylation activity. Overall, these results suggest HNRNPK methylation contributes to PRMT5-dependent AS changes that occur upon T cell activation.

T cell Trpm4 exon inclusion is controlled by PRMT5

Our data so far support that PRMT5 promotes AS changes in activated T cells that have the potential to modulate T cell biology and function. To evaluate the immunological significance of genes whose AS is regulated by PRMT5, we ran the list through the immune effector processes node (Gene Ontology [GO] identifier 0002697; Fig. 3A) in the GO knowledgebase. Immune genes whose splicing is modulated by PRMT5 corresponded to subcategories in Fc receptor signaling (GO identifier 0038093), TCR signaling (GO identifier 0050852), and regulation of T cell cytokine production (GO identifier 0002724). Within the regulation of T cell cytokine production subfamily, transient receptor potential melastatin 4 (Trpm4) was of interest in the context of our model because it has been shown to regulate Ca^{2+} signaling and IL-2 production (2). Therefore, we studied PRMT5's impact on *Trpm4* AS further.

To visualize PRMT5-dependent LSV events in *Trpm4*, we used the Voila tool within MAJIQ, which provides a Sashimi plot that shows several exon junction connections entering or leaving a reference exon. This analysis showed that our PRMT5$^{\Delta/\Delta}$ T cells have increased RNA-Seq reads for the skipping of exon 20 (61 versus 9 in PRMT5$^{fl/fl}$; Fig. 3B). This observation is better visualized in the percent spliced index (Ψ) provided by Voila. The violin plots (Fig. 3C) show the inclusion or skipping probability of *Trpm4* exon 20 in the PRMT5$^{fl/fl}$ and PRMT5$^{\Delta/\Delta}$ conditions. We observe 91.7% usage of exon 20 inclusion in the PRMT5$^{fl/fl}$ condition (Fig. 3C, left), which drops to 57% usage in the PRMT5$^{\Delta/\Delta}$ condition (Fig. 3C, right). These in silico findings were confirmed in the laboratory via semiquantitative PCR amplification, the classic method for AS validation, of a fragment encompassing exon 19 to exon 21. We observed a significant increase in the skipped product in the PRMT5-deficient condition and a significant decrease in the included/nonskipped product in the PRMT5-deficient condition (Fig. 3D, red corresponds to PRMT5-sufficient and blue to the PRMT5-deficient condition). To elucidate the biological significance of a loss of exon 20 in murine *Trpm4*, we consulted the Ensembl database. We found that the loss of exon 20 leads to nonsense-mediated decay due to an out-of-frame shift (178 bp). Based on this and the fact that there is an increase in the skipped product in the iCD4-PRMT5$^{\Delta/\Delta}$ condition, we hypothesized that there is a loss of functional TRPM4 channels in the PRMT5 KO T cells. We evaluated this by performing flow cytometry for TRPM4 in whole CD4 T cells. We observed that TRPM4^{hi} and TRPM4^{lo} populations can be observed in activated wild-type iCD4-PRMT5$^{fl/fl}$ Th cells. However, loss of PRMT5 resulted in the loss of the TRPM4^{hi} population and a significant increase in the TRPM4^{lo} population (Fig. 3E, 3F; Supplemental Fig. 3). We also note the absence of the TRPM4^{hi} population in the resting T cells (Fig. 3E, Supplemental Figure. 3). Decreases in TRPM4 mean fluorescence intensity were also observed for the TRPM4^{hi} population in PRMT5-deficient T cells (Fig. 3F). We interpret this result as the lack of PRMT5, limiting the TRPM4^{hi} population in activated CD4 T cells, is what potentially impairs T cell activation and or expansion.

PRMT5 promotes Calcium signaling, NFAT nuclear localization, and IL-2 secretion

TCR signaling induces entry of calcium (Ca^{2+}), which acts as a secondary messenger in T cell signaling pathways (40). To properly activate the transcriptional programs necessary for effective immune responses, appropriate Ca^{2+} signal amplitude and duration are necessary (41), which requires depolarization via loss of other cations. TRPM4 is a Ca^{2+} activated Na^{+} channel that permits calcium oscillation by inducing depolarization, thereby allowing sustainably elevated Ca^{2+} levels (42). Ca^{2+} in

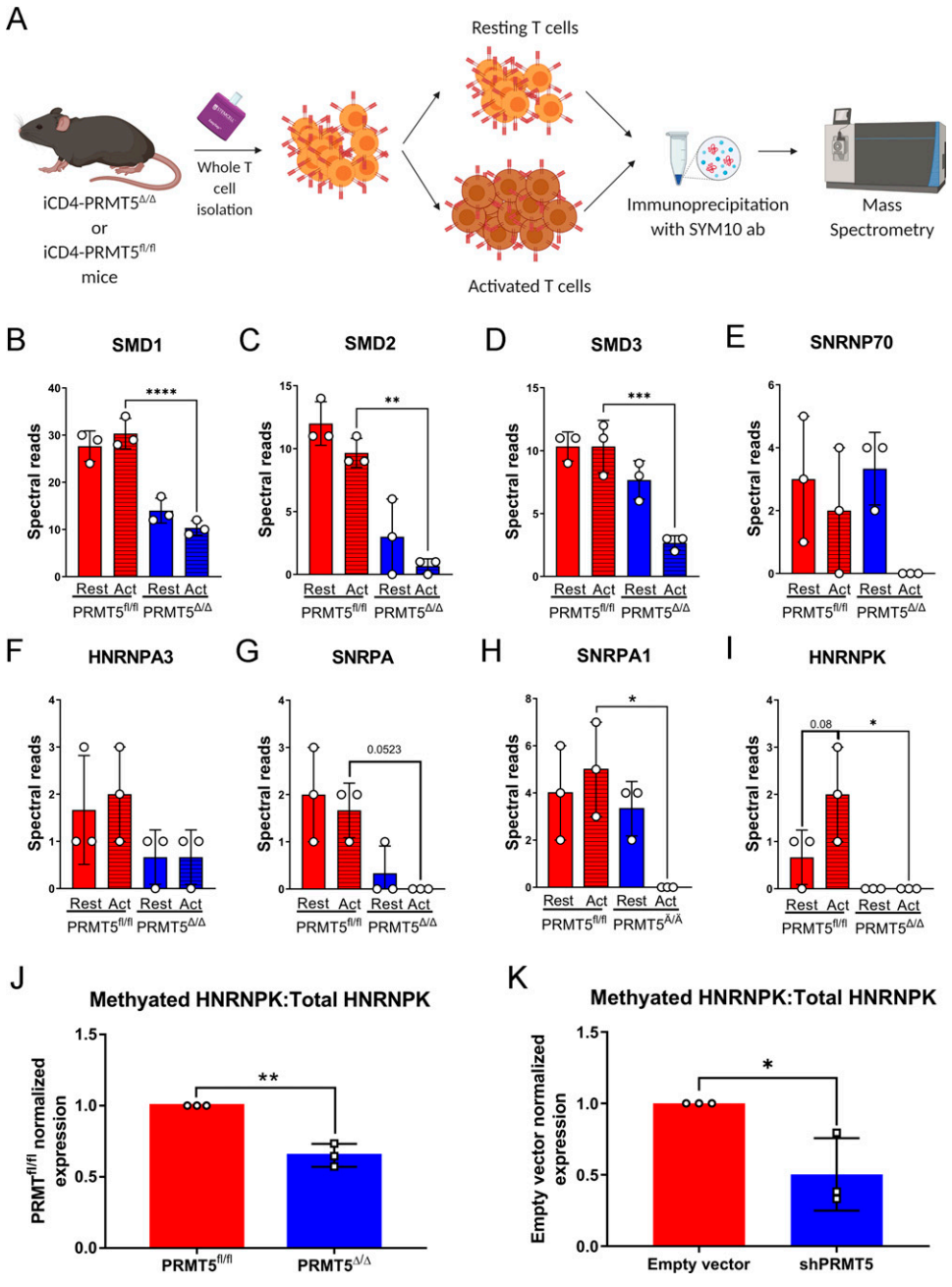

FIGURE 2. PRMT5 methylates spliceosome Sm proteins and the RNA binding protein hnRNP K.

(**A**) Experimental design for IP–MS of 48-h activated, whole $CD4^+$ T cells negative selection from iCD4-$PRMT5^{fl/fl}$ and iCD4-$PRMT5^{\Delta/\Delta}$ mice. $n = 3$ samples combined from nine age-matched mice in each respective group; IP: pan-SDM Ab SYM10. MS: LC-MS/MS. Figure created in BioRender. (**B**–**I**) SMD1 (B), SMD2 (C), SMD3 (D), SNRP70 (E), HNRNPA3 (F), SNRPA (G), SNRPA1 (H), and HNRNPK (I) MS spectral reads in protein lysates from resting and 48-h activated (act) whole $CD4^+$ T cells from iCD4-$PRMT5^{fl/fl}$ (red) and iCD4-$PRMT5^{\Delta/\Delta}$ (blue) mice after IP with the pan-SDM Ab SYM10. One-way ANOVA followed by Sidak multiple comparisons test was used. *$p < 0.05$, **$p < 0.01$, ***$p < 0.001$, ****$p < 0.0001$. Bar graphs display mean ± SD. (**J** and **K**) Quantification of methylated HNRNPK IP bands for $PRMT5^{fl/fl}$ and $PRMT5^{\Delta/\Delta}$ normalized to HNRNPK from input in 48-h activated $CD4^+$ T cells from iCD4-$PRMT5^{fl/fl}$ and iCD4-$PRMT5^{\Delta/\Delta}$ mice (J) or Jurkat T cells (K). Bar graphs display mean ± SD. $n = 3$ from three independent experiments. *$p < 0.05$, **$p < 0.01$, Student t test.

turn activates calcineurin and promotes NFAT nuclear translocation and *Il-2* gene transcription (43). If PRMT5-dependent *Trpm4* AS alters TRPM4 function, we would expect altered Ca^{2+} signaling. To study whether PRMT5 modulates the calcium signaling profile in our mouse model, we performed a 600 s trace of calcium uptake in $PRMT5^{\Delta/\Delta}$ and $PRMT5^{fl/fl}$ T cells (Fig. 4A). Cells were kept in a zero-calcium media condition and treated with the endoplasmic reticulum calcium release inhibitor thapsigargin prior to addition of Ca^{2+} to the media. This strategy provides a system to specifically study cytosolic calcium entry and plasma membrane channel response. Quantification of the "plateau" region of the trace after $CaCl_2$ addition showed that the $PRMT5^{\Delta/\Delta}$ T cells have a significant reduction in total cytosolic calcium uptake (Fig. 4B). To determine whether the expected outcome of Ca^{2+} signaling in T cells, nuclear localization of NFAT transcription complexes, was also affected, we performed NFATc1 immunocytochemistry staining. We observed a decrease in nuclear localization in the $PRMT5^{\Delta/\Delta}$ T cells (Fig. 4C; red, NFATc1; blue, DAPI). The quantification of these results confirmed a significant decrease in nuclear localization of NFATc1 in $PRMT5^{\Delta/\Delta}$ T cells (Fig.4D). Finally, it has been established that NFAT nuclear localization in activated T cells promotes the expression of IL-2, and we have previously observed decreased IL-2 after PRMT5 inhibition or

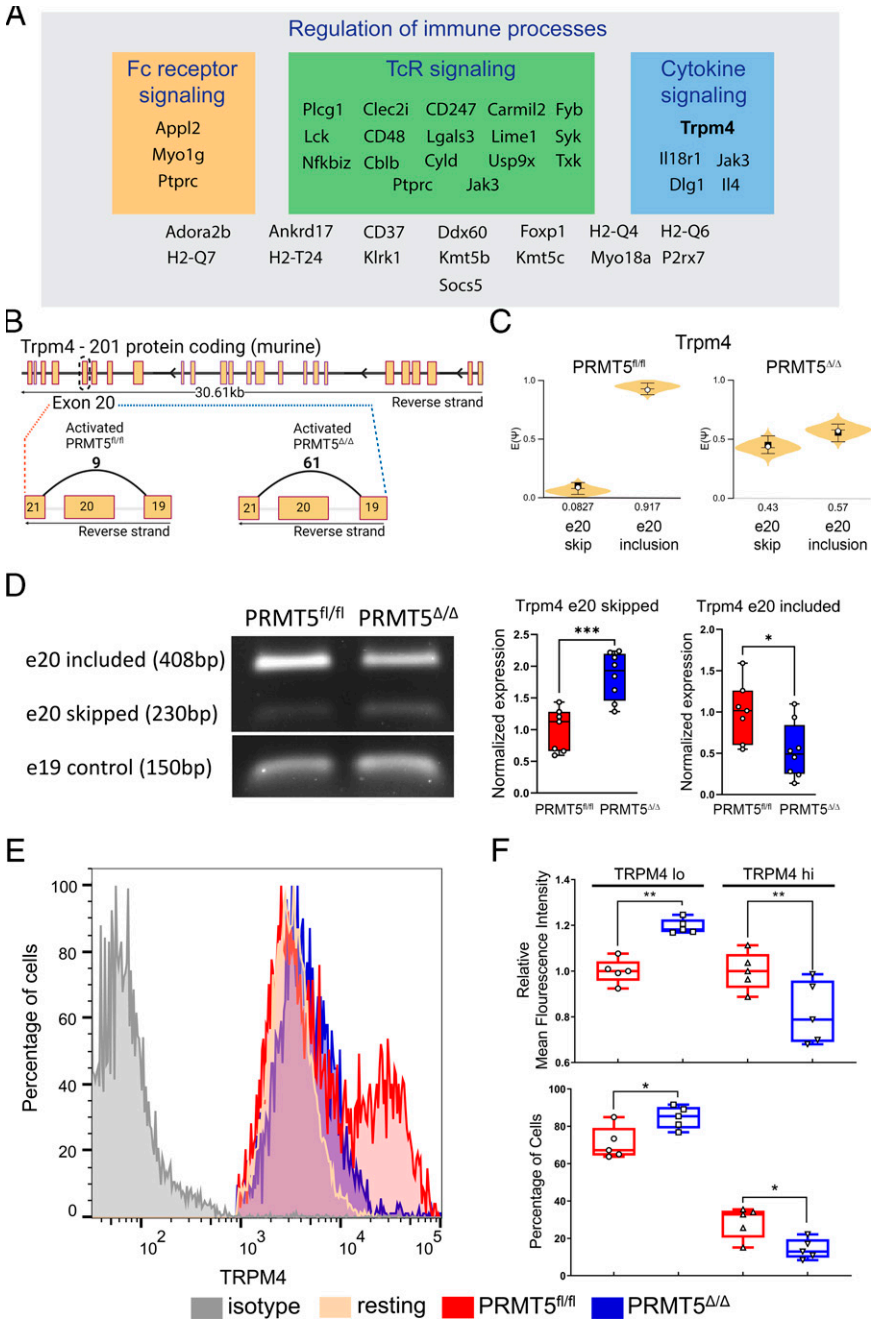

FIGURE 3. TRPM4 channel expression in T cells is affected by loss of PRMT5.

(**A**) Regulation of immune processes is a key biological term discovered from GO analysis. GO immune process genes were identified within genes whose AS was altered upon PRMT5 deletion in activated T cells. Those genes were then classified based on their GO term subgroup within immune response. We observe an overlap with genes whose AS is modulated by PRMT5, belonging to Fc receptor signaling, TCR signaling, and cytokine signaling. Grouping is based on the Panther classification system comparing against the *M. musculus* reference genome. (**B**) Protein-coding murine *Trpm4*-201 splice map. Exon 20–skipping splice graphs for PRMT5$^{fl/fl}$ and PRMT5$^{\Delta/\Delta}$ 48-h activated T cells are depicted. Numbers indicate the raw RNA-Seq reads for exon 20 skipping occurring in the two groups. Figure created in BioRender. (**C**) Violin plots from Voila shows the expected Ψ (E(Ψ)) value of *Trpm4* exon 20 skipping or inclusion in PRMT5$^{fl/fl}$ activated versus PRMT5$^{\Delta/\Delta}$ activated T cells. Ψ value is represented in a 0–1 range, indicating the probability of the AS event occurring. (**D**) Agarose gel PCR amplifying exon 19–21, showing *Trpm4* exon 20 skipping in PRMT5$^{fl/fl}$ and PRMT5$^{\Delta/\Delta}$ T cells (middle band). A section of exon 19 was used as a control product (lower band). Quantification of semiquantitative PCR assaying the PRMT5$^{fl/fl}$-normalized expression of exon 20 skipping or inclusion in PRMT5$^{fl/fl}$ and PRMT5$^{\Delta/\Delta}$ T cells. Box-and-whisker plots (points represent maximum to minimum; line represents median; box represents 25th–75th percentiles). Plots display mean ± SD. *$p < 0.05$, ***$p < 0.001$, Student *t* test. (**E**) Representative histogram overlay of TRPM4 staining in resting PRMT5$^{fl/fl}$, 48-h activated PRMT5$^{fl/fl}$, and PRMT5$^{\Delta/\Delta}$ T cells. PRMT5$^{fl/fl}$ ***(Continued)***

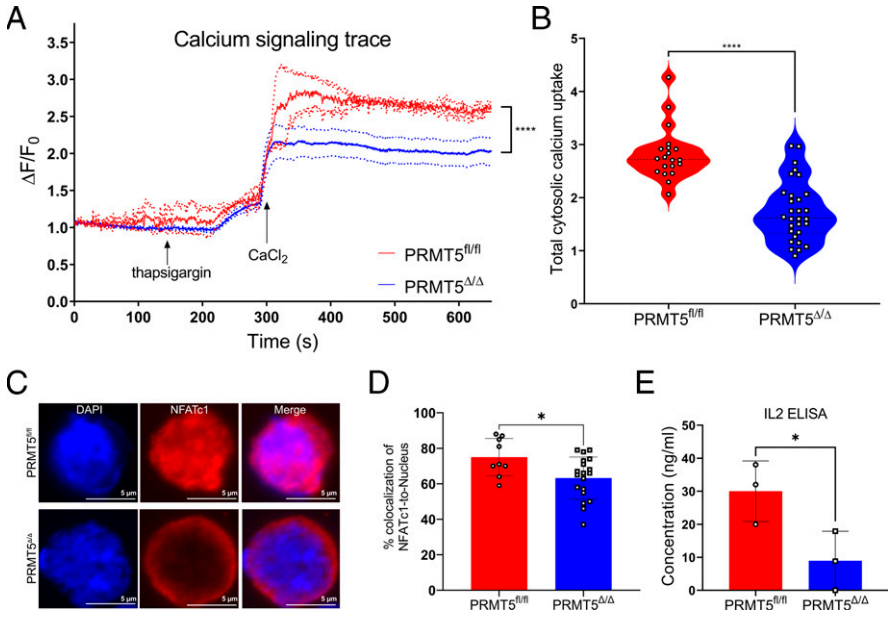

FIGURE 4. PRMT5 loss in T cells reduces calcium processivity and impacts IL-2 production.

(**A**) Live cell Fluo-4 trace studying total cytosolic calcium uptake in PRMT5$^{fl/fl}$ and PRMT5$^{\Delta/\Delta}$ T cells. PRMT5$^{\Delta/\Delta}$ T cells show a lower threshold of calcium uptake. Trace is represented as mean ± SEM, with dashed lines representing the SEM (**B**) Violin plot showing total cytosolic calcium uptake. Data points for quantification were selected from the plateau region of the trace spike after $CaCl_2$ addition. $n = 20$ time points in PRMT5$^{fl/fl}$ condition, and $n = 30$ time points in PRMT5$^{\Delta/\Delta}$ condition. Plot is displayed as mean ± SEM. Points represent maximum to minimum; line represents median. ****$p < 0.0001$, Student t test. (**C**) NFAT localization in PRMT5$^{fl/fl}$ and PRMT5$^{\Delta/\Delta}$ T cells. Clear nuclear translocation is observed in PRMT5$^{fl/fl}$ samples. Colocalization of NFAT (red) and DAPI (blue) is used to determine nuclear translocation. (**D**) Quantification of percentage colocalization of NFATc1-to-nucleus in PRMT5$^{fl/fl}$ and PRMT5$^{\Delta/\Delta}$ activated T cells, as in (C). Quantification of individual cells have been plotted, and mean and SEM were used to plot the comprehensive data. *$p < 0.05$, Student t test. (**E**) Quantification of IL-2 ELISA. ELISA was performed on supernatants from 48-h activated PRMT5$^{fl/fl}$ and PRMT5$^{\Delta/\Delta}$ T cells. Plots are displayed as mean ± SD. Points represent maximum to minimum. *$p < 0.05$, Student t test.

KO. As expected from our prior work and the role of NFAT as an IL-2 driver, PRMT5-deleted T cells secreted far less IL-2 upon T cell activation (Fig. 4E).

DISCUSSION

The main goal of this work was to explore the role of PRMT5 on AS changes in T cells and identify methylation targets of PRMT5 in T cells. We find that PRMT5 symmetrically dimethylates several proteins involved in RNA processing, including SMDs and HNRNPK, and is required for a portion of the AS pattern induced by T cell activation. We additionally found that PRMT5 modulates the splicing of a sodium channel that modulates calcium processivity, namely *Trpm4*, and promotes NFAT signaling and IL-2 production in Th cells (Fig. 5).

A substantial contribution of AS to gene expression changes induced by T cell activation was initially recognized in 2007 (13, 15). More recently, it has been shown that a number of AS changes in activated T cells translate to differential protein isoform expression and changes in T cell function (16, 44, 45). T cell activation-dependent AS changes impact genes that modulate a range of T cell processes, from signaling, migration, or fate decisions, to proliferation (15, 19, 46). We have previously shown that PRMT5 induction after T cell activation (4) promotes activation-induced cell cycle progression (12) and proliferation (2, 3). The MAJIQ analyses of PRMT5-sufficient and -deficient T cells in the current work show that PRMT5 controls ~16% of T cell activation-induced AS shifts. Such shifts occurred in genes involved in TCR, Fc receptor, and cytokine signaling, as well as other immune processes. In addition, we provide evidence that control of AS by PRMT5 is active in primary murine T cells in which loss of PRMT5 impacts T cell proliferation, NFAT signaling, and IL-2 secretion. Although our work does correlatively link these processes, future work will need to demonstrate whether specific AS changes in specific genes are necessary and/or sufficient to influence function.

T cells are indicated in red, and PRMT5$^{\Delta/\Delta}$ T cells are in blue. Isotype control is denoted in gray and resting cells are in peach. PRMT5$^{\Delta/\Delta}$ resting T cells (data not shown) had a similar peak to PRMT5$^{fl/fl}$ T cells. (**F**) Relative mean fluorescence intensity and percentage of cells depicting TRPM4^{lo} and TRPM4^{hi} peaks in PRMT5$^{fl/fl}$ and PRMT5$^{\Delta/\Delta}$ T cells. Box-and-whisker plots (points represent maximum to minimum; line represents median; box represents 25th–75th percentiles). Plots display mean ± SD. *$p < 0.05$, **$p < 0.01$, one-way ANOVA, followed by Sidak multiple comparisons test.

https://doi.org/10.4049/immunohorizons.2100076

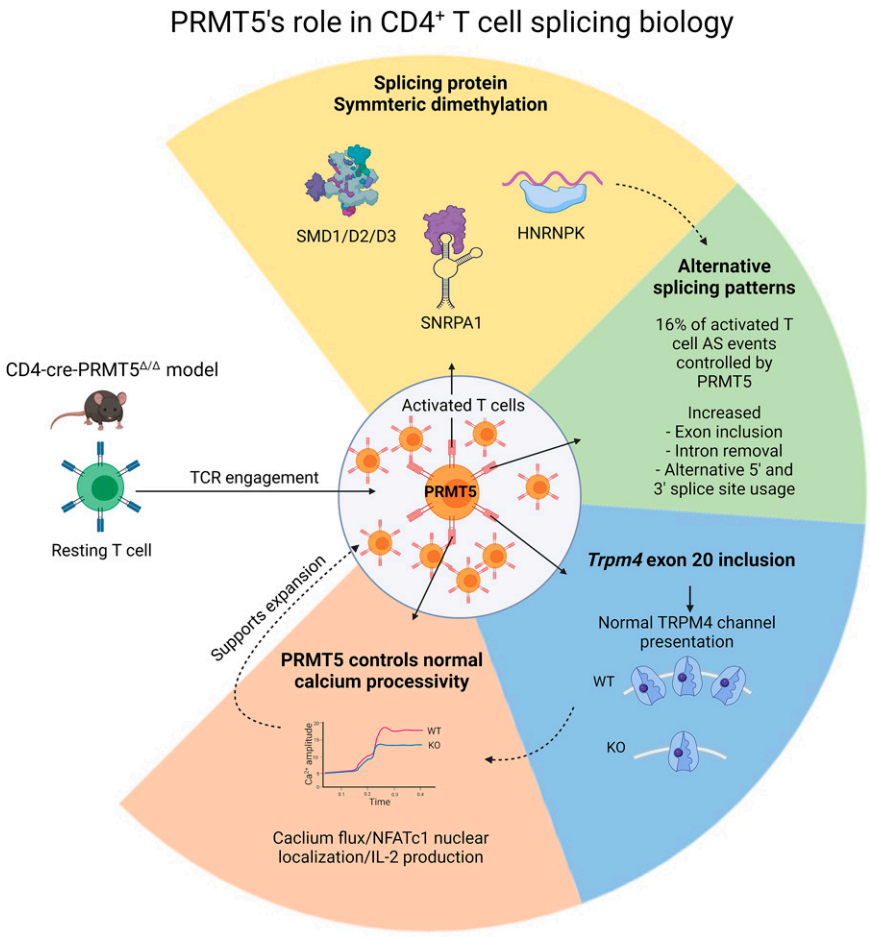

FIGURE 5. Model representing PRMT5's role in CD4⁺ T cell splicing biology.
Wedges represent the effects of activated T cell PRMT5 on symmetric dimethylation (SDM) of RNA processing proteins (yellow), alternative splicing patterns in T cells (green), Trpm4 exon inclusion status plus functional outcome (blue) and Ca2+/NFAT signaling/IL-2 production (peach). Figure created in Biorender.

The contribution of PRMT5 to AS was first recognized in plants (26). Since then, the role of PRMT5 in splicing has been studied in hematopoietic stem cells (47), neural stem/progenitor cells (28), monocytic leukemia cells (48), and murine glioma cells (31), among others. These studies evidenced that PRMT5-mediated splicing is crucial in modulating DNA repair genes (47) and MDM4 (28) and avoiding intron retention (31, 48). Metz et al. (49) studied the impact of PRMT5 small molecule inhibitors in human T cell splicing and concluded that a global reduction in SDM levels altered the splicing of a limited set of mRNA transcripts and selectively prevented TCR and pattern recognition receptor–dependent upregulation of *IFNB1* and *IFNL1*. We now show the extent to which genetic loss of PRMT5 controls splicing and find that PRMT5 controls a substantial portion of TCR-induced AS changes. As Metz et al. (49) found, not all mRNAs in our dataset appear to require PRMT5 for processing. How exactly this is achieved is currently unknown. However, TCR-induced splicing has been shown to be highly dependent on CELF2 induction and binding to specific mRNA sites (17, 46, 50), leading to the intriguing possibility that interactions between PRMT5 and CELF2 may contribute to selective splicing regulation of a group of transcripts required for activated T cell function.

We observe significantly less SMD1, SMD2, SMD3 and SNRPA1 methylation in activated PRMT5-deficient T cells. Sm proteins were the first identified methylation targets of PRMT5 that modulate RNA processing. Specifically, SMD1, SMD3, SMB, and SMB′ were found to be SDM on RG motifs by PRMT5. Methylated Sm proteins then bind SMN and accelerate U snRNP assembly (21, 24, 25, 51). Therefore, PRMT5 appears to regulate early stages of spliceosomal assembly, during SMN binding and Sm ring formation. We also observe a significant loss of SDM of HNRNPK with PRMT5 loss in mouse activated T cells. hnRNPs are involved in RNA metabolism processes, such as mRNA export, localization, stability and translation (52). hnRNPA1 methylation by PRMT5 promotes internal ribosome entry site–dependent translation of CCND1, MYC, HIF1a, and ESR1 genes (53). Additional work is now showing that hnRNPs modulate AS of pyruvate kinase isozyme splicing (54), insulin receptor gene splicing (55), CD45 AS (56), and regulate innate immunity gene control in macrophages (57). Although further work demonstrating that methylated HNRNPK mediates the observed AS changes will be necessary, our data suggest a role for HNRNPK methylation in PRMT5-dependent AS changes observed in T cells.

We found and validated *Trpm4* as an AS target of PRMT5 that is, as a consequence, substantially repressed at the protein

level in PRMT5-deficient activated T cells. The TRPM family of channels is expressed in several immune cells (58), where it controls cell proliferation, survival, and cytokine production (59). Although research on how TRPM4 contributes to T cell Ca^{2+} release, NFAT signaling and IL-2 secretion have yielded contradictory results (42, 59), we observe reductions of all three parameters in PRMT5 $^{\Delta/\Delta}$ T cells. We hypothesize this is due to reduced TRPM4, leading to lower calcium processivity. This finding could be important to explore when targeting ion channels to treat autoimmune neuroinflammation. Given the fact that the lower levels of calcium lead to reduced NFATc1 nuclear localization, it is exciting to consider whether PRMT5 inhibition could be an efficient approach to modulating overactive T cell subsets.

In summary, our work shows that PRMT5 is an important mediator of TCR-induced AS in T cells and suggests that altered methylation in splicing proteins and changes in Ca^{2+}/NFAT signaling underlie TCR expansion defects in PRMT5-deficient T cells. Additional studies will be needed to conclusively demonstrate the contribution of specific PRMT5-dependent AS changes to concrete T cell and disease phenotypes. This work and future studies may guide development of drugs targeting these processes and provide benefit to patients with autoimmune and other T cell–mediated diseases.

DISCLOSURES

M.G.-d.-A. is listed as an inventor in a pending patent of PRMT5 inhibitors and has a licensing deal with Prelude Therapeutics. The other authors have no financial conflicts of interest.

ACKNOWLEDGMENTS

We thank the Genomic Services Laboratory of the Abigail Wexner Research Institute at Nationwide Children's Hospital for help with RNA sequencing (RNA-Seq). We thank Amy Wetzel, Shireen Woodiga, Anthony Miller, and Saranga Wijeratne of the Genomic Services Laboratory at the Abigail Wexner Research Institute at Nationwide Children's Hospital, Columbus, Ohio, for help with sample quality control, library preparation, RNA-Seq, and analysis of data. We thank Liwen Zhang and Sophie Harvey from the Genomics Shared Resource at The Ohio State University for help with mass spectrometry and analysis of data.

REFERENCES

1. Müller, A. J., O. Filipe-Santos, G. Eberl, T. Aebischer, G. F. Späth, and P. Bousso. 2012. CD4+ T cells rely on a cytokine gradient to control intracellular pathogens beyond sites of antigen presentation. *Immunity* 37: 147–157.
2. Webb, L. M., S. A. Amici, K. A. Jablonski, H. Savardekar, A. R. Panfil, L. Li, W. Zhou, K. Peine, V. Karkhanis, E. M. Bachelder, et al. 2017. PRMT5- Selective inhibitors suppress inflammatory t cell responses and experimental autoimmune encephalomyelitis. [Published erratum appears in 2017 *J. Immunol.* 15: 30004] *J. Immunol.* 198: 1439–1451.
3. Webb, L. M., S. Sengupta, C. Edell, Z. L. Piedra-Quintero, S. A. Amici, J. N. Miranda, M. Bevins, A. Kennemer, G. Laliotis, P. N. Tsichlis, and M. Guerau-de-Arellano. 2020. Protein arginine methyltransferase 5 promotes cholesterol biosynthesis-mediated Th17 responses and autoimmunity. *J. Clin. Invest.* 130: 1683–1698.
4. Webb, L. M., J. Narvaez Miranda, S. A. Amici, S. Sengupta, G. Nagy, and M. Guerau-de-Arellano. 2019. NF-κB/mTOR/MYC axis drives PRMT5 protein induction after T cell activation via transcriptional and non-transcriptional mechanisms. *Front. Immunol.* 10: 524.
5. Sengupta, S., A. Kennemer, K. Patrick, P. Tsichlis, and M. Guerau-de-Arellano. 2020. Protein arginine methyltransferase 5 in T lymphocyte biology. *Trends Immunol.* 41: 918–931.
6. Smith-Garvin, J. E., G. A. Koretzky, and M. S. Jordan. 2009. T cell activation. *Annu. Rev. Immunol.* 27: 591–619.
7. Wange, R. L. 2000. LAT, the linker for activation of T cells: a bridge between T cell-specific and general signaling pathways. *Sci. STKE* 2000: re1.
8. Northrop, J. P., S. N. Ho, L. Chen, D. J. Thomas, L. A. Timmerman, G. P. Nolan, A. Admon, and G. R. Crabtree. 1994. NF-AT components define a family of transcription factors targeted in T-cell activation. *Nature* 369: 497–502.
9. Lanzavecchia, A., G. Iezzi, and A. Viola. 1999. From TCR engagement to T cell activation: a kinetic view of T cell behavior. *Cell* 96: 1–4.
10. Chow, C.-W., M. Rincón, and R. J. Davis. 1999. Requirement for transcription factor NFAT in interleukin-2 expression. *Mol. Cell. Biol.* 19: 2300–2307.
11. Gullberg, M., and K. A. Smith. 1986. Regulation of T cell autocrine growth. T4+ cells become refractory to interleukin 2. *J. Exp. Med.* 163: 270–284.
12. Amici, S. A., W. Osman, and M. Guerau-de-Arellano. 2021. PRMT5 promotes cyclin E1 and cell cycle progression in CD4 Th1 cells and correlates with EAE severity. *Front. Immunol.* 12: 695947.
13. Martinez, N. M., Q. Pan, B. S. Cole, C. A. Yarosh, G. A. Babcock, F. Heyd, W. Zhu, S. Ajith, B. J. Blencowe, and K. W. Lynch. 2012. Alternative splicing networks regulated by signaling in human T cells. *RNA* 18: 1029–1040.
14. Black, D. L. 2003. Mechanisms of alternative pre-messenger RNA splicing. *Annu. Rev. Biochem.* 72: 291–336.
15. Ip, J. Y., A. Tong, Q. Pan, J. D. Topp, B. J. Blencowe, and K. W. Lynch. 2007. Global analysis of alternative splicing during T-cell activation. *RNA* 13:563–572.
16. Agosto, L. M., M. R. Gazzara, C. M. Radens, S. Sidoli, J. Baeza, B. A. Garcia, and K. W. Lynch. 2019. Deep profiling and custom databases improve detection of proteoforms generated by alternative splicing. *Genome Res.* 29: 2046–2055.
17. Mallory, M. J., S. J. Allon, J. Qiu, M. R. Gazzara, I. Tapescu, N. M. Martinez, X.-D. Fu, and K. W. Lynch. 2015. Induced transcription and stability of CELF2 mRNA drives widespread alternative splicing during T-cell signaling. *Proc. Natl. Acad. Sci. USA* 112: E2139–E2148.
18. Shankarling, G., B. S. Cole, M. J. Mallory, and K. W. Lynch. 2014. Transcriptome-wide RNA interaction profiling reveals physical and functional targets of hnRNP L in human T cells. *Mol. Cell. Biol.* 34: 71–83.
19. Martinez, N. M., L. Agosto, J. Qiu, M. J. Mallory, M. R. Gazzara, Y. Barash, X. D. Fu, and K. W. Lynch. 2015. Widespread JNK-dependent alternative splicing induces a positive feedback loop through CELF2-mediated regulation of MKK7 during T-cell activation. *Genes Dev.* 29: 2054–2066.
20. Boisvert, F.-M., J. Cote, M.-C. Boulanger, P. Cleroux, F. Bachand, C. Autexier, and S. Richard. 2002. Symmetrical dimethylarginine methylation is required for the localization of SMN in Cajal bodies and pre-mRNA splicing. *J. Cell Biol.* 159: 957–969.
21. Friesen, W. J., S. Massenet, S. Paushkin, A. Wyce, and G. Dreyfuss. 2001. SMN, the product of the spinal muscular atrophy gene, binds

preferentially to dimethylarginine-containing protein targets. *Mol. Cell* 7: 1111–1117.
22. Gonsalvez, G. B., L. Tian, J. K. Ospina, F.-M. Boisvert, A. I. Lamond, and A. G. Matera. 2007. Two distinct arginine methyltransferases are required for biogenesis of Sm-class ribonucleoproteins. *J. Cell Biol.* 178: 733–740.
23. Brahms, H., J. Raymackers, A. Union, F. de Keyser, L. Meheus, and R. Lührmann. 2000. The C-terminal RG dipeptide repeats of the spliceosomal Sm proteins D1 and D3 contain symmetrical dimethylarginines, which form a major B-cell epitope for anti-Sm autoantibodies. *J. Biol. Chem.* 275: 17122–17129.
24. Friesen, W. J., S. Paushkin, A. Wyce, S. Massenet, G. S. Pesiridis, G. Van Duyne, J. Rappsilber, M. Mann, and G. Dreyfuss. 2001. The methylosome, a 20S complex containing JBP1 and pICln, produces dimethylarginine-modified Sm proteins. *Mol. Cell. Biol.* 21: 8289–8300.
25. Meister, G., C. Eggert, D. Bühler, H. Brahms, C. Kambach, and U. Fischer. 2001. Methylation of Sm proteins by a complex containing PRMT5 and the putative U snRNP assembly factor pICln. *Curr. Biol.* 11: 1990–1994.
26. Deng, X., L. Gu, C. Liu, T. Lu, F. Lu, Z. Lu, P. Cui, Y. Pei, B. Wang, S. Hu, and X. Cao. 2010. Arginine methylation mediated by the *Arabidopsis* homolog of PRMT5 is essential for proper pre-mRNA splicing. *Proc. Natl. Acad. Sci. USA* 107: 19114–19119.
27. Sanchez, S. E., E. Petrillo, E. J. Beckwith, X. Zhang, M. L. Rugnone, C. E. Hernando, J. C. Cuevas, M. A. Godoy Herz, A. Depetris-Chauvin, C. G. Simpson, et al. 2010. A methyl transferase links the circadian clock to the regulation of alternative splicing. *Nature* 468: 112–116.
28. Bezzi, M., S. X. Teo, J. Muller, W. C. Mok, S. K. Sahu, L. A. Vardy, Z. Q. Bonday, and E. Guccione. 2013. Regulation of constitutive and alternative splicing by PRMT5 reveals a role for Mdm4 pre-mRNA in sensing defects in the spliceosomal machinery. *Genes Dev.* 27: 1903–1916.
29. Koh, C. M., M. Bezzi, D. H. P. Low, W. X. Ang, S. X. Teo, F. P. H. Gay, M. Al-Haddawi, S. Y. Tan, M. Osato, A. Sabò, et al. 2015. MYC regulates the core pre-mRNA splicing machinery as an essential step in lymphomagenesis. *Nature* 523: 96–100.
30. Hamard, P.-J., G. E. Santiago, F. Liu, D. L. Karl, C. Martinez, N. Man, A. K. Mookhtiar, S. Duffort, S. Greenblatt, R. E. Verdun, and S. D. Nimer. 2018. PRMT5 regulates DNA repair by controlling the alternative splicing of histone-modifying enzymes. *Cell Rep.* 24: 2643–2657.
31. Braun, C. J., M. Stanciu, P. L. Boutz, J. C. Patterson, D. Calligaris, F. Higuchi, R. Neupane, S. Fenoglio, D. P. Cahill, H. Wakimoto, et al. 2017. Coordinated splicing of regulatory detained introns within oncogenic transcripts creates an exploitable vulnerability in malignant glioma. *Cancer Cell* 32: 411–426.e11.
32. Vaquero-Garcia, J., A. Barrera, M. R. Gazzara, J. González-Vallinas, N. F. Lahens, J. B. Hogenesch, K. W. Lynch, and Y. Barash. 2016. A new view of transcriptome complexity and regulation through the lens of local splicing variations. *eLife* 5: e11752.
33. Ponnalagu, D., S. Gururaja Rao, J. Farber, W. Xin, A. T. Hussain, K. Shah, S. Tanda, M. Berryman, J. C. Edwards, and H. Singh. 2016. Molecular identity of cardiac mitochondrial chloride intracellular channel proteins. *Mitochondrion* 27: 6–14.
34. Liu, H., R. G. Sadygov, and J. R. Yates III. 2004. A model for random sampling and estimation of relative protein abundance in shotgun proteomics. *Anal. Chem.* 76: 4193–4201.
35. Urlaub, H., V. A. Raker, S. Kostka, and R. Lührmann. 2001. Sm protein-Sm site RNA interactions within the inner ring of the spliceosomal snRNP core structure. *EMBO J.* 20: 187–196.
36. Chiou, N., and K. W. Lynch. 2014. Mechanisms of Spliceosomal Assembly. In *Spliceosomal Pre-mRNA Splicing: Methods and Protocols: Methods in Molecular Biology* K. J. Hertel ed. Humana Press, Totowa, NJ. p. 35–43.
37. Price, S. R., P. R. Evans, and K. Nagai. 1998. Crystal structure of the spliceosomal U2B″-U2A' protein complex bound to a fragment of U2 small nuclear RNA. *Nature* 394: 645–650.
38. Ma, A. S. W., K. Moran-Jones, J. Shan, T. P. Munro, M. J. Snee, K. S. Hoek, and R. Smith. 2002. Heterogeneous nuclear ribonucleoprotein A3, a novel RNA trafficking response element-binding protein. *J. Biol. Chem.* 277: 18010–18020.
39. Geuens, T., D. Bouhy, and V. Timmerman. 2016. The hnRNP family: insights into their role in health and disease. *Hum. Genet.* 135: 851–867.
40. Samakai, E., C. Go, and J. Soboloff. 2018. Defining the Roles of Ca2+ Signals during T Cell Activation. In *Signaling Mechanisms Regulating T Cell Diversity and Function.* J. Soboloff, and D. J. Kappes, eds. CRC Press/Taylor & Francis, Boca Raton, FL. p. 177–202
41. Dolmetsch, R. E., R. S. Lewis, C. C. Goodnow, and J. I. Healy. 1997. Differential activation of transcription factors induced by Ca2+ response amplitude and duration. *Nature* 386: 855–858.
42. Launay, P., A. Fleig, A.-L. Perraud, A. M. Scharenberg, R. Penner, and J.-P. Kinet. 2002. TRPM4 is a Ca2+-activated nonselective cation channel mediating cell membrane depolarization. *Cell* 109: 397–407.
43. Clipstone, N. A., and G. R. Crabtree. 1992. Identification of calcineurin as a key signalling enzyme in T-lymphocyte activation. *Nature* 357: 695–697.
44. Martinez, N. M., and K. W. Lynch. 2013. Control of alternative splicing in immune responses: many regulators, many predictions, much still to learn. *Immunol. Rev.* 253: 216–236.
45. Radens, C. M., D. Blake, P. Jewell, Y. Barash, and K. W. Lynch. 2020. Meta-analysis of transcriptomic variation in T-cell populations reveals both variable and consistent signatures of gene expression and splicing. *RNA* 26: 1320–1333.
46. Ajith, S., M. R. Gazzara, B. S. Cole, G. Shankarling, N. M. Martinez, M. J. Mallory, and K. W. Lynch. 2016. Position-dependent activity of CELF2 in the regulation of splicing and implications for signal-responsive regulation in T cells. *RNA Biol.* 13: 569–581.
47. Tan, D. Q., Y. Li, C. Yang, J. Li, S. H. Tan, D. W. L. Chin, A. Nakamura-Ishizu, H. Yang, and T. Suda. 2019. PRMT5 modulates splicing for genome integrity and preserves proteostasis of hematopoietic stem cells. *Cell Rep.* 26: 2316–2328.e6.
48. Radzisheuskaya, A., P. V. Shliaha, V. Grinev, E. Lorenzini, S. Kovalchuk, D. Shlyueva, V. Gorshkov, R. C. Hendrickson, O. N. Jensen, and K. Helin. 2019. PRMT5 methylome profiling uncovers a direct link to splicing regulation in acute myeloid leukemia. *Nat. Struct. Mol. Biol.* 26: 999–1012.
49. Metz, P. J., K. A. Ching, T. Xie, P. Delgado Cuenca, S. Niessen, J. H. Tatlock, K. Jensen-Pergakes, and B. W. Murray. 2020. Symmetric arginine dimethylation is selectively required for mRNA splicing and the initiation of type I and type III interferon signaling. *Cell Rep.* 30: 1935–1950.e8.
50. Mallory, M. J., S. P. McClory, R. Chatrikhi, M. R. Gazzara, R. J. Ontiveros, and K. W. Lynch. 2020. Reciprocal regulation of hnRNP C and CELF2 through translation and transcription tunes splicing activity in T cells. *Nucleic Acids Res.* 48: 5710–5719.
51. Friesen, W. J., A. Wyce, S. Paushkin, L. Abel, J. Rappsilber, M. Mann, and G. Dreyfuss. 2002. A novel WD repeat protein component of the methylosome binds Sm proteins. *J. Biol. Chem.* 277: 8243–8247.
52. Dreyfuss, G., V. N. Kim, and N. Kataoka. 2002. Messenger-RNA-binding proteins and the messages they carry. *Nat. Rev. Mol. Cell Biol.* 3: 195–205.
53. Gao, G., S. Dhar, and M. T. Bedford. 2017. PRMT5 regulates IRES-dependent translation via methylation of hnRNP A1. *Nucleic Acids Res.* 45: 4359–4369.

54. Clower, C. V., D. Chatterjee, Z. Wang, L. C. Cantley, M. G. Vander Heiden, and A. R. Krainer. 2010. The alternative splicing repressors hnRNP A1/A2 and PTB influence pyruvate kinase isoform expression and cell metabolism. *Proc. Natl. Acad. Sci. USA* 107: 1894–1899.
55. Talukdar, I., S. Sen, R. Urbano, J. Thompson, J. R. Yates III, and N. J. G. Webster. 2011. hnRNP A1 and hnRNP F modulate the alternative splicing of exon 11 of the insulin receptor gene. *PLoS One* 6: e27869.
56. Topp, J. D., J. Jackson, A. A. Melton, and K. W. Lynch. 2008. A cell-based screen for splicing regulators identifies hnRNP LL as a distinct signal-induced repressor of CD45 variable exon 4. *RNA* 14: 2038–2049.
57. West, K. O., H. M. Scott, S. Torres-Odio, A. P. West, K. L. Patrick, and R. O. Watson. 2019. The splicing factor hnRNP M is a critical regulator of innate immune gene expression in macrophages. *Cell Rep.* 29: 1594–1609.e5.
58. Bertin, S., and E. Raz. 2016. Transient receptor potential (TRP) channels in T cells. *Semin. Immunopathol.* 38: 309–319.
59. Weber, K. S., K. Hildner, K. M. Murphy, and P. M. Allen. 2010. Trpm4 differentially regulates Th1 and Th2 function by altering calcium signaling and NFAT localization. *J. Immunol.* 185: 2836–2846.